Pergamon

Int. J. Solids Structures Vol. 33, No. 24, pp. 3517–3538, 1996

0020-7683/96 $15.00 + .00

0020-7683(95)00195-6

FURTHER EXPERIMENTAL INVESTIGATION ON THE ECCENTRICITY FACTOR IN THE PROGRESSIVE CRUSHING OF TUBES

A. A. SINGACE
Mechanical Engineering Dept., College of Engineering, University of Bahrain, P.O. Box 32038, Manama, Bahrain

and

H. ELSOBKY
Mechanical Engineering Department, UMIST, P.O. Box 88, Manchester M60 1QD, UK

(*Received* 6 *April* 1995; *in revised form* 15 *July* 1995)

Abstract—In an earlier work by Singace *et al.* [Singace, A. A., ElSobky, H. and Reddy, T. Y. (1994). On the eccentricity factor in the progressive crushing of tubes. *Int. J. Solids. Struct.* **32**, 3589–3602] an attempt was made to experimentally validate the eccentricity factor, m, in the progressive crushing of tubes. The test was made on an aluminium tube of a D/t ratio ≈ 31. This paper experimentally investigates the effect of the D/t ratio and the tube material on the value of m given theoretically by 0.65. The values of the inward and the outward folding angles, denoted by α_0 and β_0 respectively, were also evaluated. Good agreement was obtained between the experimental values and those produced by the analysis. Influence of strain hardening was evident on the value of m. Copyright © 1996 Elsevier Science Ltd.

1. INTRODUCTION

The axial progressive crushing of tubes has recently gained much attention due to its usage in the design of impact energy absorption devices. Axially crushed short tubes will deform either in the axisymmetric (concertina or ring) type fold or the non-axisymmetric (diamond or lobe) type fold depending mainly upon the tube diameter to wall thickness (D/t) ratio (Mallock, 1908; Foppl, 1926; Geckeler, 1928; Coppa, 1962; Horton *et al.*, 1966; Allan, 1968; Johnson *et al.*, 1977; Sobel and Newman, 1980; Andrews *et al.*, 1983, Abramowicz and Jones 1984, 1986). Effect of the tube length to wall thickness (L/t) and the D/t ratios on the mode of collapse was investigated by Andrews *et al.* (1983) and a classification chart relating these variables was presented. Relatively thinner tubes normally exhibit diamond type folds and thicker tubes generally deform into a concertina mode. In some cases, thin tubes start deforming into the concertina type fold before reverting to the diamond mode. Nevertheless, the opposite of such phenomenon has not been observed. This experimental study will focus only on tubes deforming into the concertina mode.

Many attempts followed Alexander's attempt (1960) to analytically evaluate the mean crushing load of an axially crushed tube deforming in the concertina mode. Some researchers implemented Alexander's kinematics collapse mechanism and focused on redefining some of the parameters used in the derivation of the mean crushing load (Johnson, 1972; Andronicou and Walker, 1981; Amdahl and Soreide, 1981). Other tried to improve Alexander's model in an attempt to produce a more realistic fold. (Wierzbicki and Bhat, 1984; Abramowicz and Jones, 1986; Grzebieta, 1990). All these models impose only a radially outward displacement of the tube wall in an attempt to achieve a more realistic fold pattern. Review of analytical models for the plastic crushing behaviour of tubes has been presented by, among others, Jones (1989) and Singace *et al.* (1994).

Experiments have shown that the wall of an axisymmetrically deformed tube will be laid down partly to the inside and partly to the outside of the tube generator, the total of which is defined by the folding length. The experiment has also shown that the outward

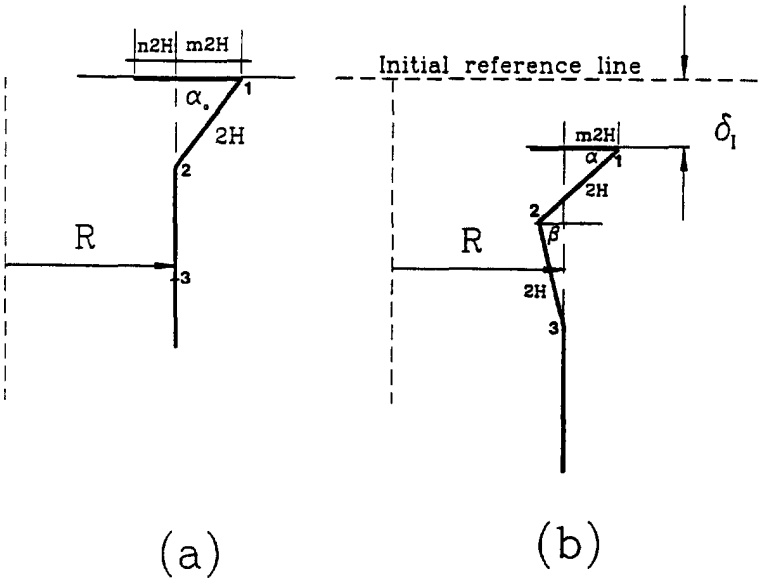

Fig. 1. The formation and progression of an inward fold: (a) critical position of an outward fold; (b) the first phase of the subsequent inward fold.

part is bigger than the inward part. The concept of the ratio of the outward part of the folding length to the total folding length was introduced by Wierzbicki *et al.* (1992). It is known by the eccentricity factor and denoted by m. The analytical model was based on a rigid perfectly-plastic material and assumes that each fold will be formed by three plastic hinges as shown in Figs 1 and 2.

A typical load-displacement curve of a tube deforming in the concertina mode is shown in Fig. 3 and is characterized by alternate high and low peak loads. These peaks, marked O and I, correspond to the formation of the outward and the inward parts of the folds and are indicated by the angles α_o and β_o respectively. The eccentricity factor, m, was found to be related to these angles, see Figs 1 and 2. In the analysis produced by Wierzbicki *et al.* (1992), m was not obtainable and arbitrary. Wierzbicki *et al.*'s model supposed that the radial distances from the plastic hinges are fixed and equal to R. Singace *et al.* (1994),

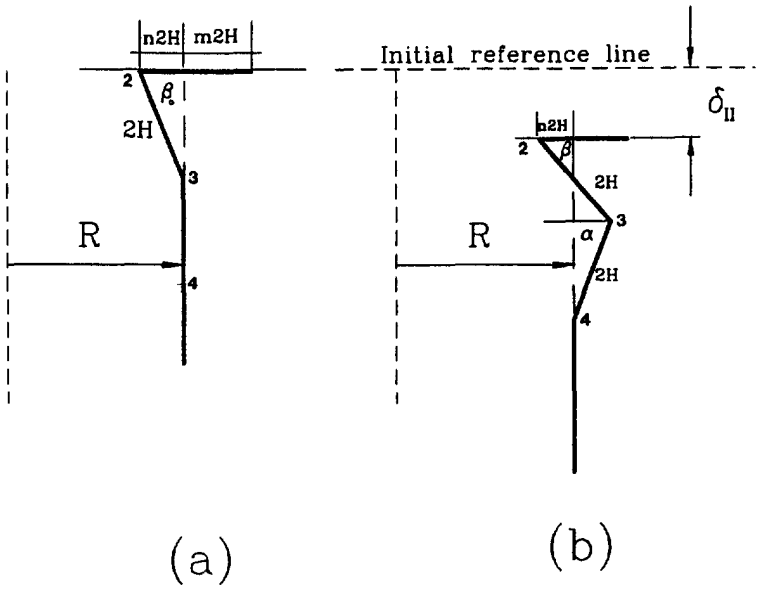

Fig. 2. The transition between the inward fold and the subsequent outward fold: (a) critical position of the inward fold; (b) the first phase of the subsequent outward fold.

Table 1a. The tubes material and their geometrical measurements (mm)

Material	Specimen label	Outside diameter	Tube thickness	Tube length
Aluminium alloy	A1127	12.7	0.7	39
	A125	24.5	1.0	102
	A150	50.8	1.6	101
	A1100	101.5	3.6	203
Brass	Br90	89	3.3	200
Copper	Cua30	29	1.63	51
	Cun50	52.5	1.6	102.4
	Cua50	51	3.0	102.3
Mild steel	Ms50	52	1.5	102.5

Table 1b. Some properties of the tube materials

Tube material	Yield stress (MPa)	Ultimate stress (MPa)	Strain at ultimate stress (%)	Strain at fracture (%)
Aluminium alloy (HT30) annealed	46.5	134	20.5	24.1
Copper (C106) As received	351	379	1.4	2
Copper (C106) Annealed	75	203	50	55
Mild steel (BS3602)	230	343	33	40

however, assumed that this distance was variable, given generally by R_i and managed to produce a discrete value for m given by 0.65. Subsequently, the values for the critical angles relating the inward and the outward fold, i.e. α_o and β_o, were also evaluated. Singace *et al.* (1994) attempted to experimentally validate the theoretical values of m, α_o and β_o using a test on 50 mm nominal diameter and 1.5 mm thick aluminum alloy tubes.

This is a purely experimental work and endeavours to further substantiate the theoretical findings of Singace *et al.* (1994) and investigate the effect of the tube material and its D/t ratio on the value of m. An experiment was designed to provide means of measuring the first few values of α_o and β_o for tubes of different materials and D/t ratios.

2. TESTING PROCEDURE

Eight sets of aluminum alloy (HT30), brass, copper (C106) and mild steel (BS3602) tubes, the geometrical parameters and the testing labels of which are shown in Table 1a, were axially crushed at the rate of 5 mm/min using a universal Instron testing machine. Based on the experience of the authors and others, see for example Andrews *et al.* (1983), the dimensions of the tubes were selected such that they deform in the concertina mode when axially crushed. The D/t and the L/t ratios of the tubes were in the ranges of 17–67 and 31–102, respectively.

Aluminum tubes were annealed by soaking them at 360°C for half an hour and then allowing them to cool in the furnace. Copper and mild steel tubes were maintained at 550°C and 600°C, respectively, for half an hour then water quenched.

Tensile tests were carried out on aluminium alloy, copper and mild steel specimens of which material properties are shown in Table 1b. Annealed aluminium had an elastic strain hardening region followed by a perfectly plastic zone up to the fracture point. Received copper showed an elastic perfectly plastic behaviour while annealed copper exhibited clear strain hardening characteristics. After the upper and lower yield points, mild steel tubes exhibited a perfectly-plastic region ($\sim 2\%$ strain) before strain hardening.

The tubes were compressed to the deformation level and the peak load corresponding to the peaks O's and I's shown in Fig. 3. These peaks are related to the formation of each fold as explained earlier. The tubes were compressed in the steps to the position marked by

Table 2. The experimental results of the first five consecutive peaks* (tube set: A1127)

Peak (Fig. 6)	Load (kN)	Shortening (mm)	Critical angle (°)
Second (first outward fold)	2.44	5.45	$\alpha_o = 50$
Third (first inward fold)	3.12	6.73	$\beta_o = 67$
Fourth (second outward fold)	2.35	10.85	$\alpha_o = 48$
Fifth (second inward fold)	3.40	11.75	$\beta_o = 72$
	Value of m	0.67	
	$2H$ (mm)	3.19	

* The first peak which corresponds to the initial buckle is disregarded. Only second and subsequent peaks are considered in all the tests.

Table 3. The experimental results of the first five consecutive peaks (tube set: A125)

Peak (Fig. 7)	Load (kN)	Shortening (mm)	Critical angle (°)
Second (first outward fold)	5.0	8.94	$\alpha_o = 50$
Third (first inward fold)	6.77	12.11	$\beta_o = 70$
Fourth (second outward fold)	5.68	16.67	$\alpha_o = 50$
Fifth (second inward fold)	5.88	19.13	$\beta_o = 69$
	Value of m	0.63	
	$2H$ (mm)	3.75	

the O's and Is in each of the first five consecutive peak loads. The first peak, usually the highest, contributes in the triggering of progressive crushing and cease to play further role after the critical position of the first fold has been reached. This marks the state of the alternation in the peak load shown in the previous figure. (Fig. 3). For this reason, focus on the initial peak was excluded in this study. An overview on the formation of the initial fold, based on the experimental observation, was presented by Singace *et al.* (1994). After compression, the tubes were sectioned longitudinally to carry out the dimensional measurements necessary to derive the values for m, α_o and β_o. To obtain the value of m, the curved length of the folds on either side of the original position of the tube generator was measured after magnifying the image to a reasonable scale. A typical example of a sectioned tube is shown in Fig. 4. To measure α_o and β_o, a similar approach was applied to the relevant section of the tube.

3. EXPERIMENTAL RESULTS AND DISCUSSIONS

Enlarged images of selected tubes of different materials are shown in Fig. 5. These figures show critical angles, α_o and β_o, which correspond to three consecutive outward and two consecutive inward folds for the aluminium alloy, brass and copper tubes. The cross-sectional views of the deformed tubes and the corresponding load–displacement characteristics for the aluminium alloy, copper and mild steel tubes are shown in Figs 6–13. In each tube compression test, a load–displacement curve is produced, and in order to minimize the number of graphs, only one typical curve is shown. However, the positions at which the load interruption of each tube occurs exhibited in Fig 6b–13b, are shown in the load-displacement curves in Figs 6a–13a.

The measured values of α_o and β_o for each crushed tube and the overall value of m in each set are tabulated in Tables 2–10. The corresponding peak loads and the tube end shortening measurements are also included in the same tables. Table 11 shows the average of these values and are compared with the theoretical predictions by Singace *et al.* (1994). The angles measured are consistent with the theoretical values given by eqns (1) and (10) of Singace *et al.* (1994). These angles are respectively given by:

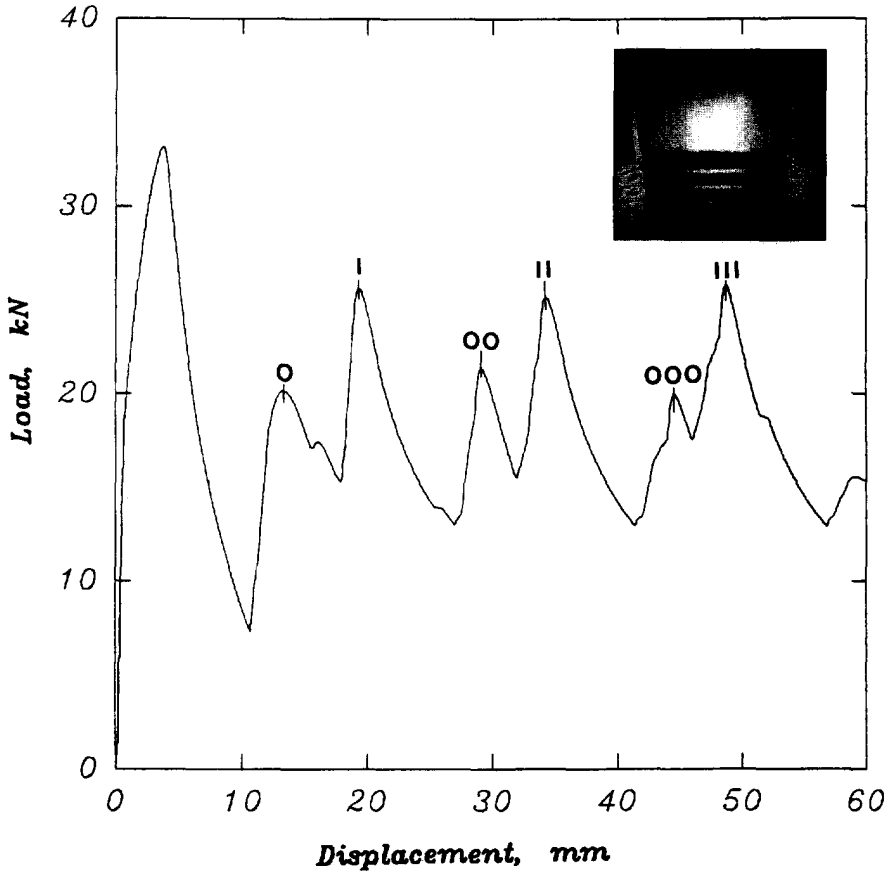

Fig. 3. The load-deflection curve of the axial compression test of an aluminium alloy tube 50.8 mm outside the diameter and 1.6 mm thickness (concertina mode). Inset is the tube compressed up to the fourth inward fold.

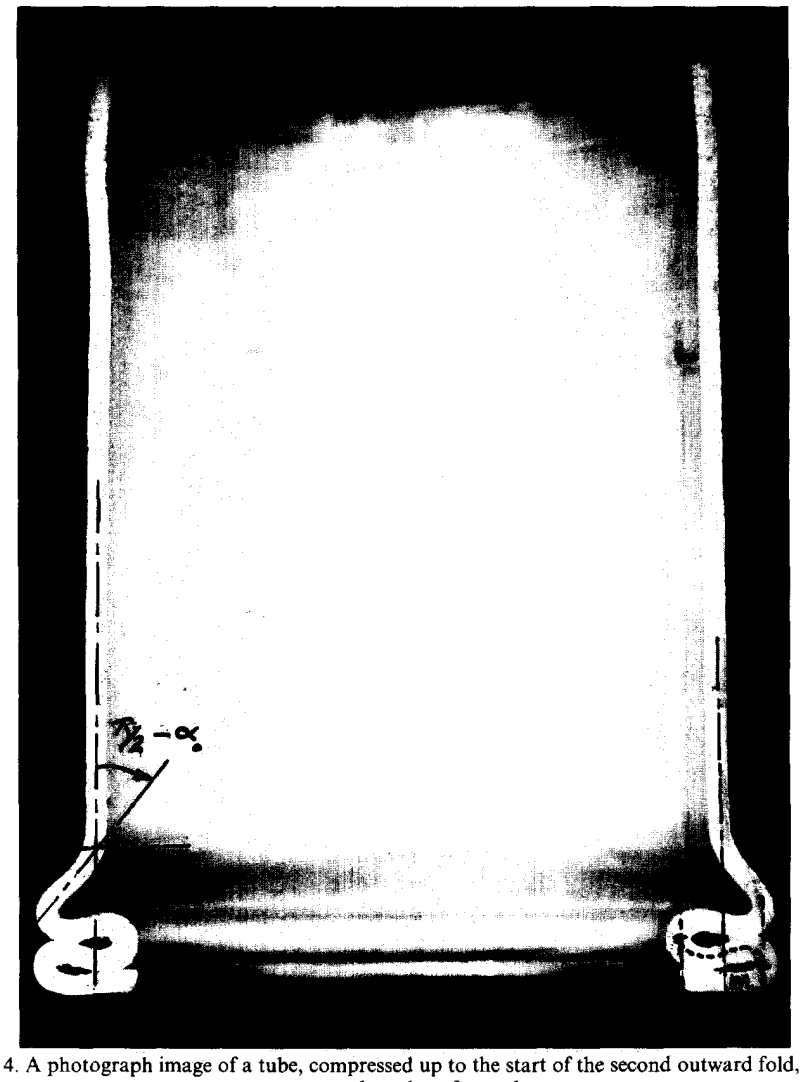

Fig. 4. A photograph image of a tube, compressed up to the start of the second outward fold, used to extract the value of m and α_o.

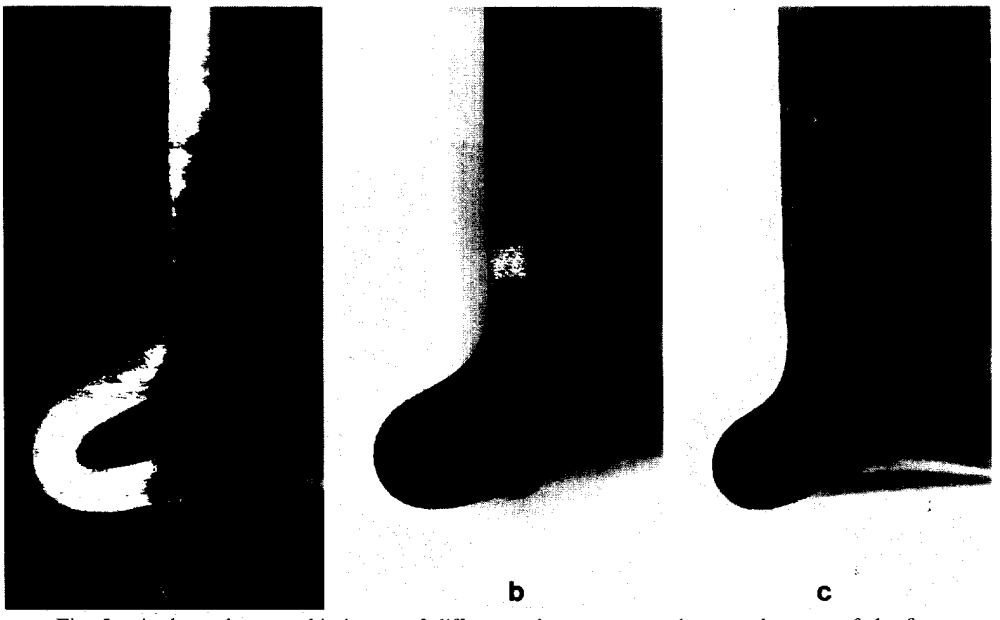

Fig. 5a. A close photographic image of different tubes, compressed up to the start of the first outward fold, used to extract the value of α_o corresponding to the peak (O) in Fig. 3. (a) Aluminium tube (A1100), (b) brass tube (Br90), (c) copper tube (Cua50).

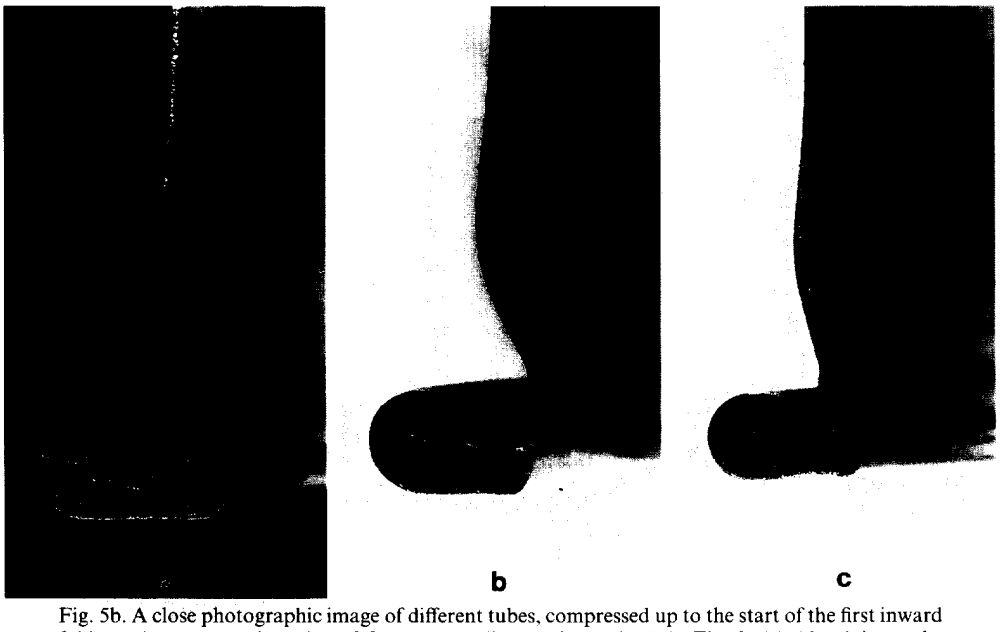

Fig. 5b. A close photographic image of different tubes, compressed up to the start of the first inward fold, used to extract the value of β_o corresponding to the peak (I) in Fig. 3. (a) Aluminium tube (A1100), (b) brass tube (Br90), (c) copper tube (Cua50).

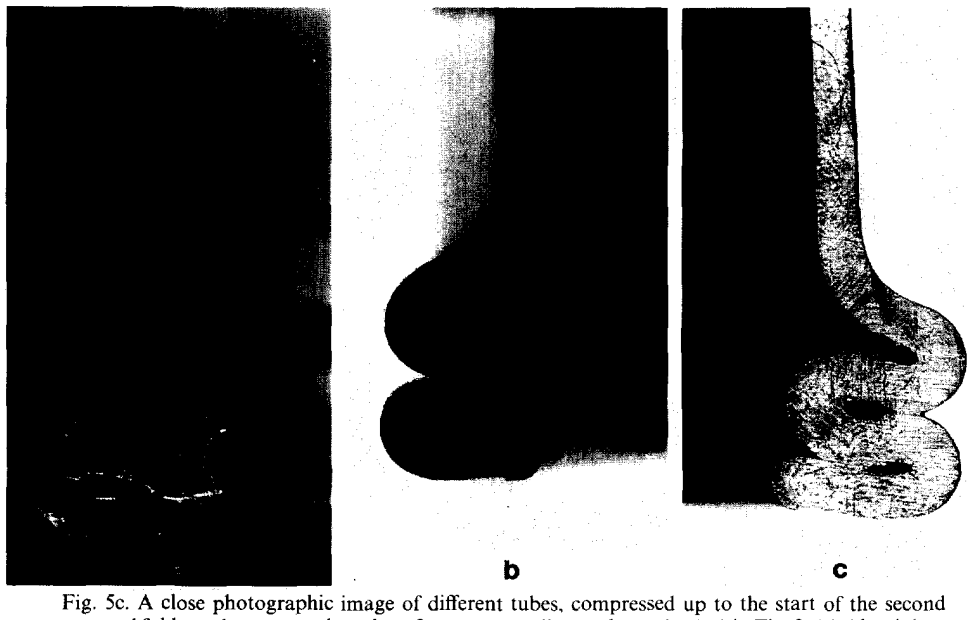

Fig. 5c. A close photographic image of different tubes, compressed up to the start of the second outward fold, used to extract the value of α_o corresponding to the peak (*OO*) in Fig. 3. (a) Aluminium tube (A1100), (b) brass tube (Br90), (c) copper tube (Cua50).

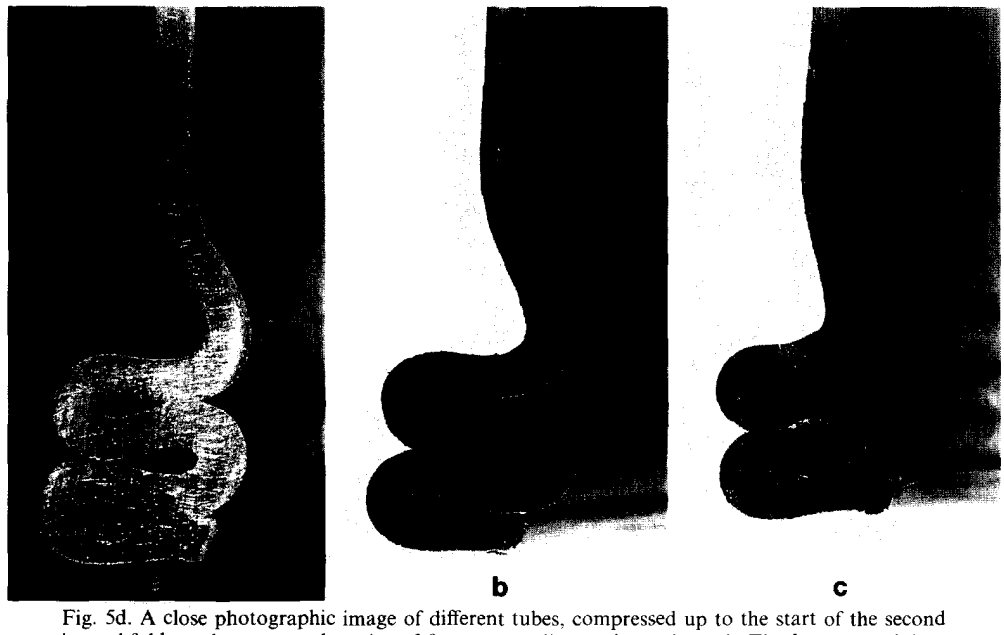

Fig. 5d. A close photographic image of different tubes, compressed up to the start of the second inward fold, used to extract the value of β_o corresponding to the peak (*II*) in Fig. 3. (a) Aluminium tube (A1100), (b) brass tube (Br90), (c) copper tube (Cua50).

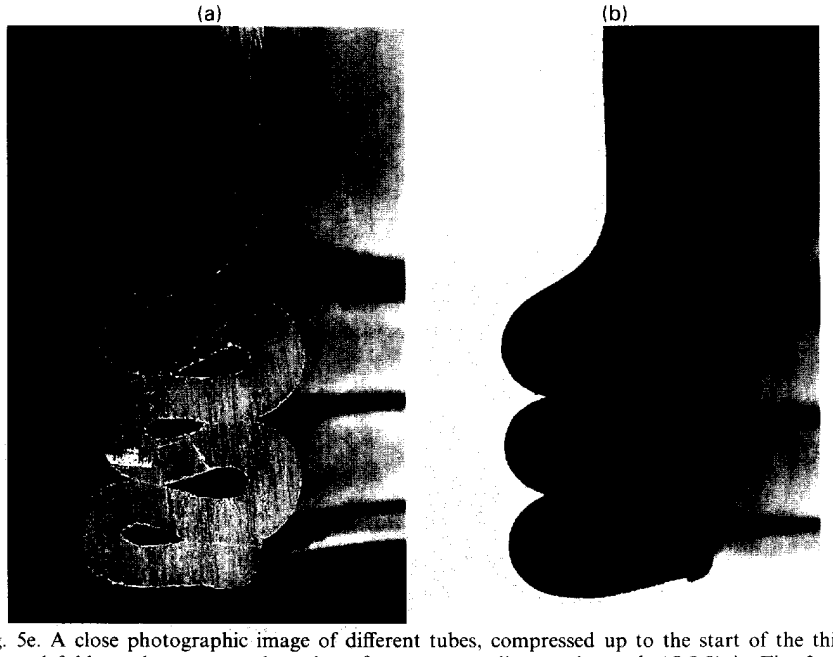

Fig. 5e. A close photographic image of different tubes, compressed up to the start of the third outward fold, used to extract the value of α_u corresponding to the peak (*OOO*) in Fig. 3. (a) Aluminium tube (A1100), (b) brass tube (Br90).

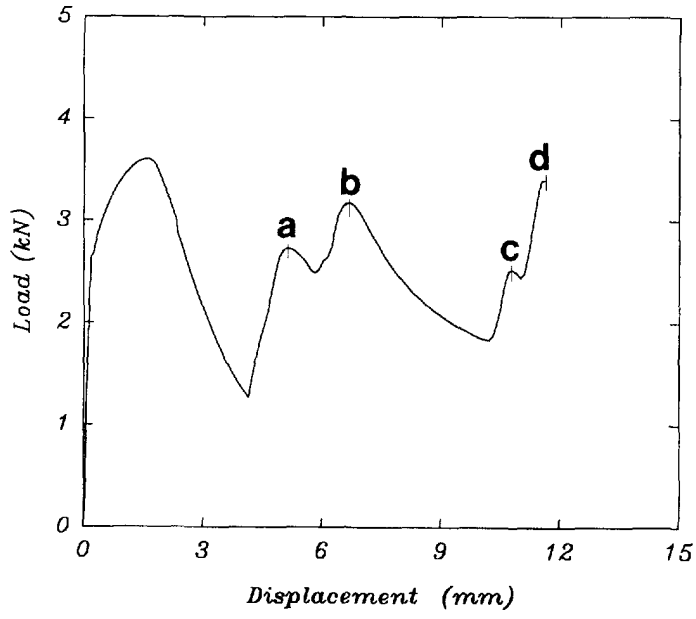

Fig. 6a. The load-deflection curve of the axial compression test of an aluminium alloy tube (A1127) of 12.7 mm outside diameter and 0.7 mm wall thickness.

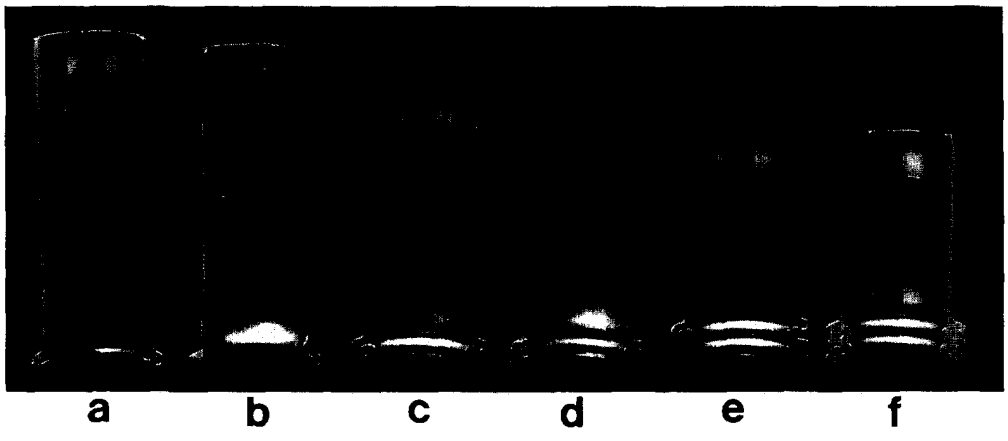

Fig. 6b. Photographs showing the aluminium tube deformed up to the start of: (a) the first outward fold, (b) the first inward fold, (c) the second outward fold, (d) the second inward fold, (e) the third incomplete outward fold, (f) the third inward fold.

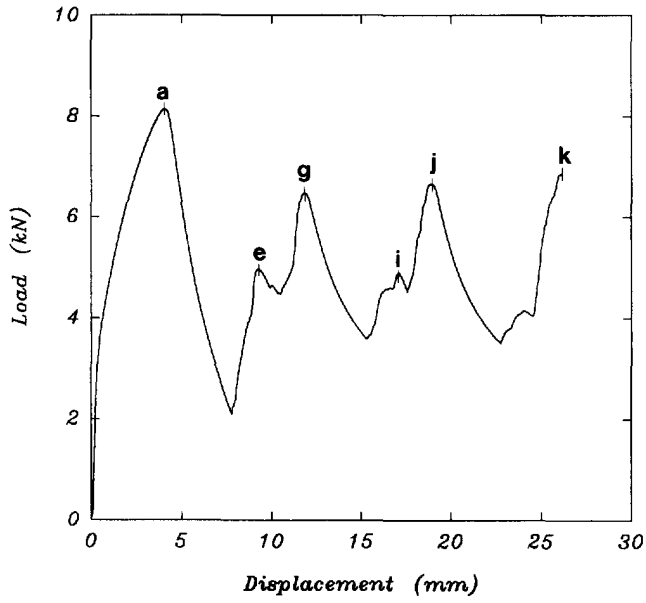

Fig. 7a. The load-deflection curve of the axial compression test of an aluminium alloy tube (A125) of 24.5 mm outside diameter and 1.0 mm wall thickness.

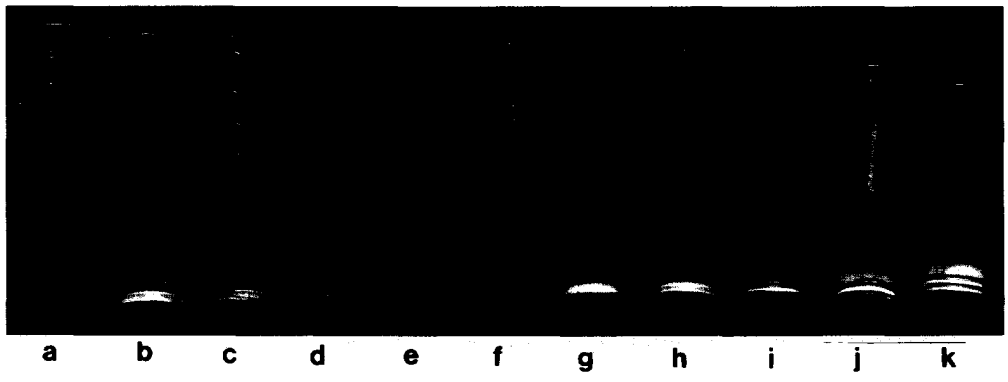

Fig. 7b. Photographs showing the aluminium tube deformed up to the start of: (e) the first outward fold, (g) the first inward fold, (i) the second fold, (j) the second inward fold, (k) the third inward fold.

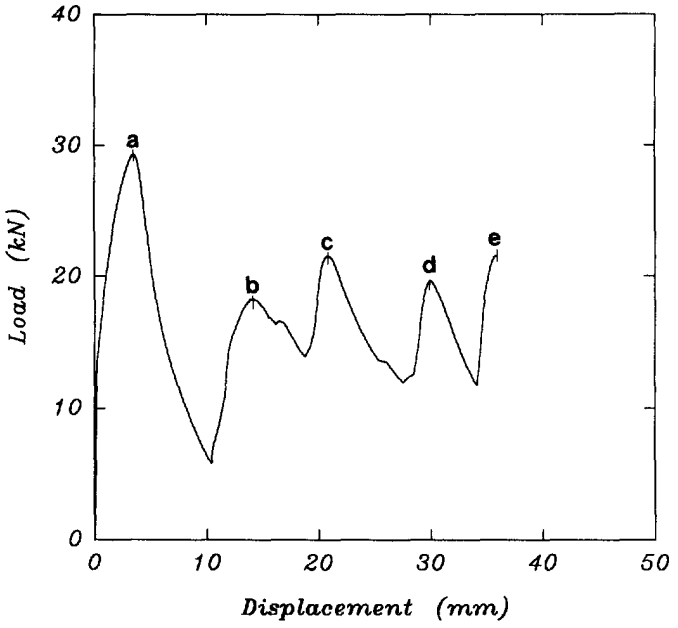

Fig. 8a. The load-deflection curve of the axial compression test of an aluminium alloy tube (A150) of 50.8 mm outside diameter and 1.6 mm wall thickness.

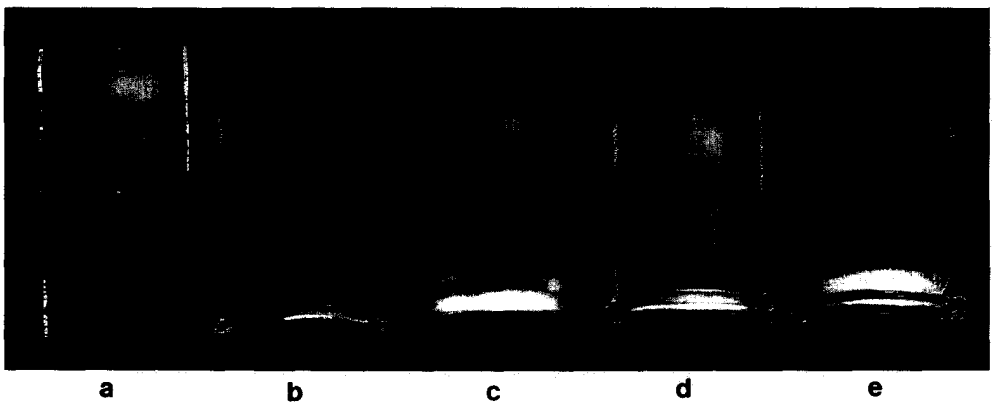

Fig. 8b. Photographs showing the aluminium tube deformed up to the start of: (b) the first outward fold, (c) the first inward fold, (d) the second outward fold, (e) the second inward fold.

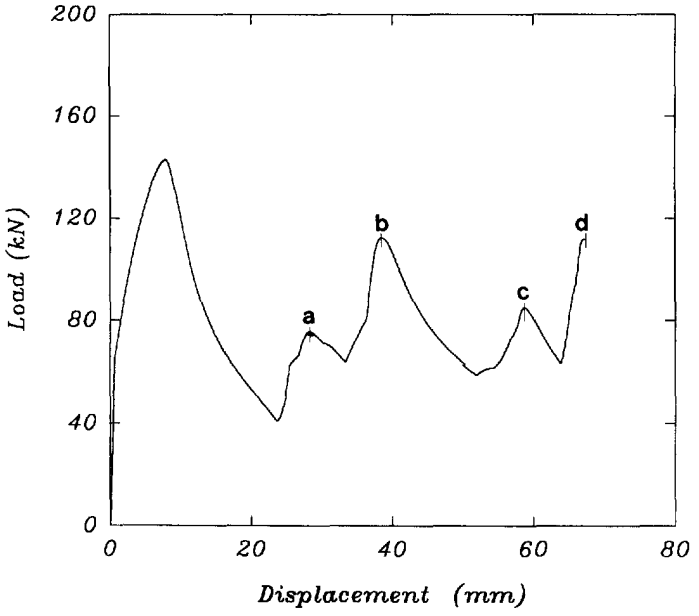

Fig. 9a. The load-deflection curve of the axial compression test of an aluminium alloy tube (A1100) of 100.5 mm outside diameter and 3.6 mm wall thickness.

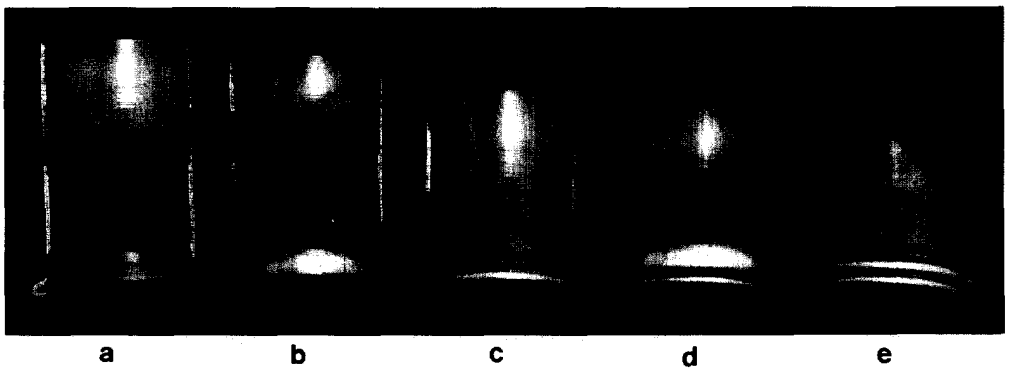

Fig. 9b. Photographs showing the aluminium tube deformed up to the start of: (a) the first outward fold, (b) the first inward fold, (c) second outward fold, (d) the second inward fold, (e) the third outward fold.

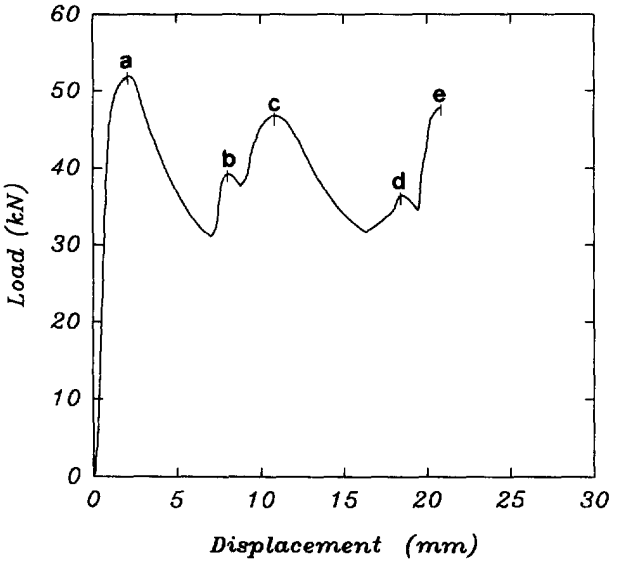

Fig. 10a. The load-deflection curve of the axial compression test of the annealed copper tube (Can 30) of 29 mm outside diameter and 1.63 mm wall thickness.

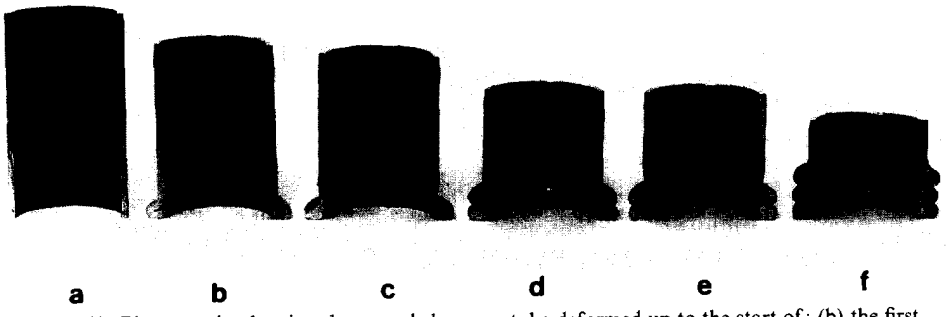

Fig. 10b. Photographs showing the annealed copper tube deformed up to the start of: (b) the first outward fold, (c) the first inward fold, (d) the second outward fold, (e) the second inward fold, (f) the third outward fold.

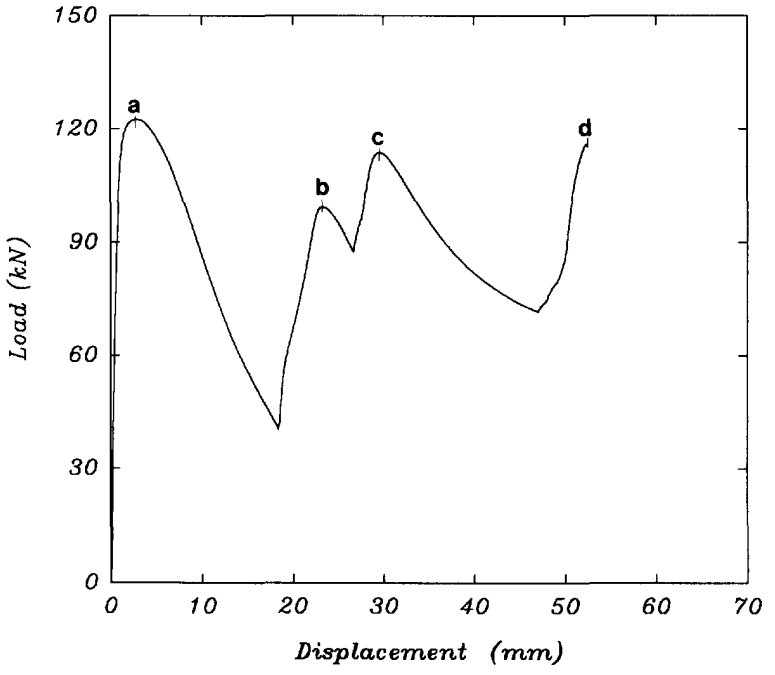

Fig. 11a. The load-deflection curve of the axial compression test of as-received copper alloy tube (Cua50) of 51 mm outside diameter and 3 mm wall thickness.

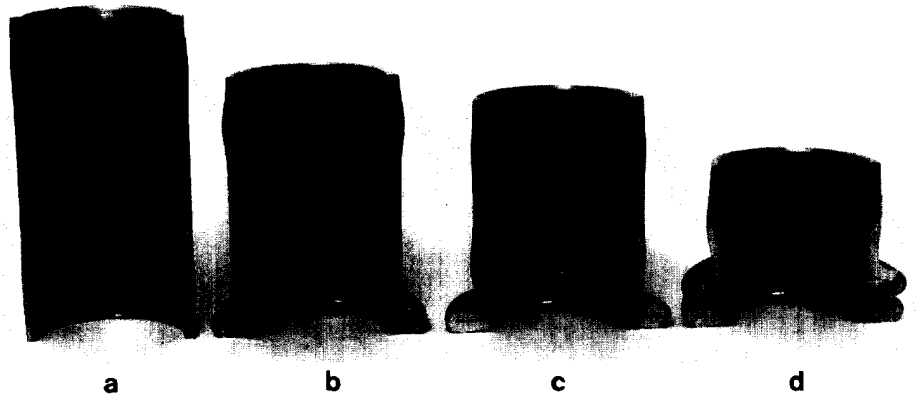

Fig. 11b. Photographs showing the as-received copper tube deformed up to the start of: (b) the first outward fold, (c) the first inward fold, (d) the second inward fold.

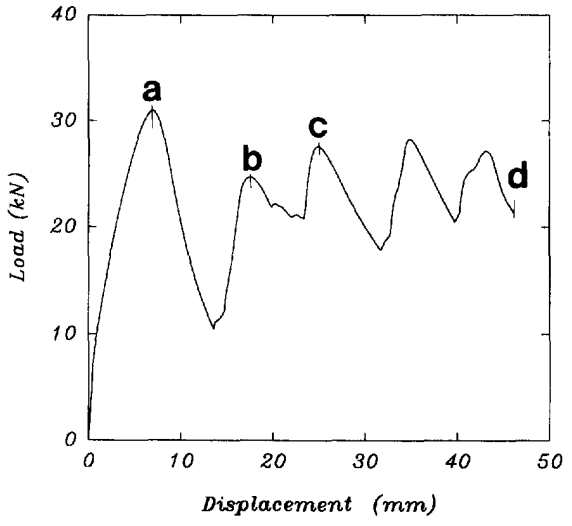

Fig. 12a. The load-deflection curve of the axial compression test of an annealed copper tube (Can50) of 52.5 mm outside diameter and 1.6 mm wall thickness.

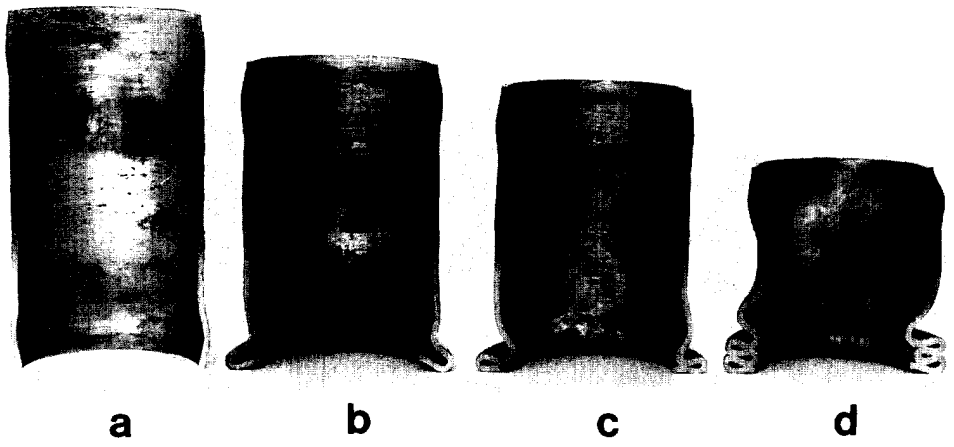

Fig. 12b. Photographs showing the annealed copper tube deformed up to the start of: (b) the first outward fold, (c) the first inward fold, (d) start of change of mode.

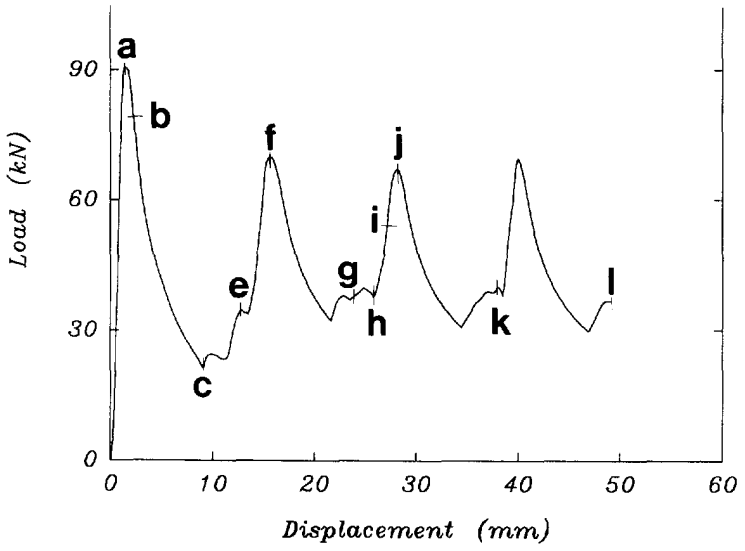

Fig. 13a. The load-deflection curve of the axial compression test of a mild steel tube (Ms50) of 52 mm outside diameter and 1.5 mm wall thickness.

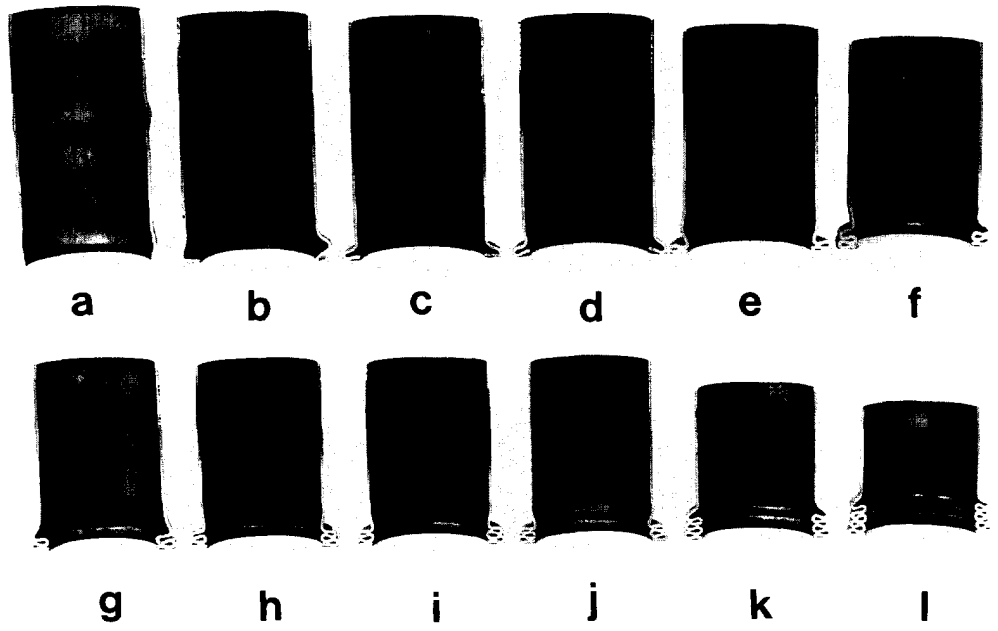

Fig. 13b. Photographs showing the mild steel tube deformed up to the start of: (c) the first outward fold, (e) the first inward fold, (g) the second outward fold, (j) the second outward fold, (k) the third outward fold, (i) fourth outward fold.

Table 4. The experimental results of the first five consecutive peaks (tube set : A150)

Peak (Fig. 8)	Load (kN)	Shortening (mm)	Critical angle ( )
Second (first outward fold)	20.44	12.77	$\alpha_o = 50$
Third (first inward fold)	25.69	19.52	$\beta_o = 68$
Fourth (second outward fold)	22.06	27.27	$\alpha_o = 49$
Fifth (second inward fold)	21.56	35.27	$\beta_o = 69$
	Value of m	0.60	
	$2H$ (mm)	8.17	

Table 5. The experimental results of the first five consecutive peaks (tube set : A1100)

Peak (Fig. 9)	Load (kN)	Shortening (mm)	Critical angle ( )
Second (first outward fold)	71.59	28.64	$\alpha_o = 45$
Third (first inward fold)	105.52	39.42	$\beta_o = 70$
Fourth (second outward fold)	82.28	61.32	$\alpha_o = 47$
Fifth (second inward fold)	111.84	68	$\beta_o = 70$
	Value of m	0.59	
	$2H$ (mm)	17	

Table 6. The experimental results of the first five consecutive peaks (tube set : Br90)

Peak*	Load (kN)	Shortening (mm)	Critical angle ( )
Second (first outward fold)	231	22	$\alpha_o = 50$
Third (first inward fold)	252	34.3	$\beta_o = 68.5$
Fourth (second outward fold)	224	55	$\alpha_o = 50$
Fifth (second inward fold)	263	62	$\beta_o = 69$
	Value of m	0.62	
	$2H$ (mm)	16.5	

* These specimens were tested on a machine which does not have the capability of data conversion and transfer.

Table 7. The experimental results of the first five consecutive peaks (tube set: Cua30)

Peak (Fig. 10)	Load (kN)	Shortening (mm)	Critical angle ( )
Second (first outward fold)	102.5	22.60	$\alpha_o = 50$
Third (first inward fold)	111.53	30.02	$\beta_o = 70$
Fourth (second outward fold)	91.8	51.58	$\alpha_o = 50$
Fifth (second inward fold)	115.89	52.48	$\beta_o = 70.5$
	Value of m	0.61	
	$2H$ (mm)	12.15	

Table 8. The experimental results of the first five consecutive peaks (tube set : Cua50)

Peak (Fig. 11)	Load (kN)	Shortening (mm)	Critical angle ( )
Second (first outward fold)	35.22	8.76	$\alpha_o = 50$
Third (first inward fold)	46.90	11.50	$\beta_o = 70$
Fourth (second outward fold)	33.91	19.60	$\alpha_o = 50$
Fifth (second inward fold)	47.84	20.84	$\beta_o = 71$
	Value of m	0.64	
	$2H$ (mm)	5.1	

Table 9. The experimental results of the first five consecutive peaks (tube set: Cun50)

Peak (Fig. 12)	Load (kN)	Shortening (mm)	Critical angle (°)
Second (first outward fold)	22.50	18.50	$\alpha_o = 49$
Third (first inward fold)	28.38	25.00	$\beta = 66$
Fourth (second outward fold)	21.84	38.10	*
Fifth (second inward fold)	27.5	43.00	*
	Value of m	0.59	
	$2H$ (mm)	10.75	

* Transition to lobed mode

Table 10. The experimental results of the first six consecutive peaks (tube set: Ms50)

Peak (Fig. 13)	Load (kN)	Shortening (mm)	Critical angle (°)
Second (first outward fold)	36.54	11.23	$\alpha_o = 50$
Third (first inward fold)	53.75	17.08	$\beta_o = 70$
Fourth (second outward fold)	44.73	23.74	$\alpha_o = 50$
Fifth (second inward fold)	63.91	27.50	$\beta_o = 70$
Sixth (third outward fold)	44.29	39.83	$\alpha_o = 50$
	Value of m	0.60	
	$2H$ (mm)	7.5	

Table 11. The experimental and the theoretical values of m, $2H$, α_o and β_o of the axially crushed tubes

Specimen label	Geometrical ratios		Eccentricity ratio m		Inward critical α_o		Outward critical β_o		Fold length $2H$	
	D/t	L/t	Expt	theory	Expt	eqn (1)	Expt	eqn (2)	Expt	eqn (3)
A1127	18.14	55.71	0.67	0.65	49	49.62	69.5	69.38	3.19	2.64
A125	24.5	102	0.63	0.65	50	49.62	69.5	69.38	3.75	4.39
A150	31.75	63.13	0.60	0.65	46.5	49.62	69.5	69.38	8.17	7.99
A1100	28.19	56.39	0.59	0.65	46	49.62	70	69.38	17	16.94
Br90	26.97	60.61	0.62	0.65	50	49.62	69	69.38	16.5	15.19
Cua30	17.19	31.29	0.64	0.65	50	49.62	70.50	69.38	5.1	6.09
Cun50	32.81	64	0.59	0.65	49	49.62	69.0	69.38	10.75	8.12
Cua50	17	34.1	0.61	0.65	50	49.62	70.25	69.38	12.15	10.96
Ms50	34.67	68.33	0.60	0.65	50	49.62	70	69.38	7.5	7.83

$$\alpha_o = \cos m \tag{1}$$

$$\beta_o = 1 - \cos m \tag{2}$$

Inserting the theoretical value of m, given by 0.65, into eqns (1) and (2), the theoretical values of the critical outward and inward angles, α_o and β_o are, respectively given by 49.62 and 69.38. The values of the folding length, denoted by $2H$, are also shown in these tables and compared with the theoretical values given by (Singace *et al.*, 1994); eq.(30) of the same reference)

$$H = \sqrt{\frac{\pi R t}{8}} \tag{3}$$

where R and t are the mean tube radius and wall thickness respectively.

While the measured critical angles, α_o and β_o, corresponding to the critical position of the outward and inward fold respectively, are in excellent agreement with the theoretical values, the value of m, obtained from the analysis and equal to 0.65, is slightly higher than the average measured reading of 0.62. This is mainly attributed to the fact that the theoretical model implemented by Singace *et al.* (1994) was based on stationary plastic hinges lobed at the end of the straight-line elements which does not virtually correspond to the experimental

observation. A better agreement between the theory and the practice is expected if a continuous zone, or curved elements are used to represent the folding elements. This is conceivable only if strain hardening effects were taken into account, a subject that is not within the scope of this study at the present time.

Tubes which possess greater strain hardening capacity (annealed mild steel and copper) show a tendency to deform in non-axisymmetric folding mode. These tubes are generally soft. Harder material tubes (aluminium and as-received copper) which generally lack or have less strain hardening capacity deform in axisymmetric folding mode. The eccentricity factor for the first group was around 0.63 while in the second group, m was maintained at ~ 0.60. Hence, strain hardening play an important role in enhancing the value of m. Theoretical modeling of axial crushing of tubes would produce closer values of m to that from the experiment if the material strain-hardening characteristics were considered.

During the experiments, two features were noted and worthwhile mentioning. The first is the effect of heat treatment on the mode of collapse of axially crushed tubes. At some stages during the axial crushing of strain-hardened tubes like copper alloy and mild steel, which have been heat treated, a transition in the mode of collapse from the concertina mode to the diamond mode has been noted. Such a phenomenon has been experimentally studied by Reddy and Zhang (1993) who concluded that the removal of strain hardening not only changes the mode of deformation but, in some cases, causes an overall loss of stability of the crushed tubes.

The other interesting feature noted from the experiments is the rippling over the tube surface of the heated treated copper and more notably on the mild steel tubes (to the feel of the finger), Figs 12b and 13b. This phenomenon was also reported by Grzebieta (1990). Work-hardening causes the ripples to occur simultaneously and it is the end conditions which cause the tube to buckle at one of its ends, and deform further into one of the two modes.

Furthermore, the mild steel tubes showed a tendency to buckle not only at the tube ends but also at the middle length of the tube. This may also be attributed to the strain hardening characteristics of copper alloy and mild steel, Fig. 13.

4. CONCLUSIONS

Aluminium alloy, brass, copper and mild steel tubes of different D/t ratios were axially crushed to deform axisymmetrically. The crushing test was designed to stop loading at the alternate low and high peaks of a typical load-displacement curve of a crushed tube deforming into the concertina mode. These peaks correspond to inward and outward fold angles, α_o and β_o and are related to the eccentricity factor, m. This factor assumes that the tube folding length will be divided into parts; the outward and the inward in a ratio to the total length of 0.65 and 0.35 respectively. The values of α_o and β_o were in good agreement with the theoretical values irrespective of the variation in the material and the D/t ratio. Although the value of m is in a reasonably good agreement with that produced by the theory, the experiment showed that m is slightly sensitive to the strain hardening characteristics of the compressed tube material. A theoretical model using curved elements and a proper flow rule is expected to produce a value for m closer to that obtained from the experiment.

REFERENCES

Abramowicz, W. and Jones, N. (1984). Dynamic axial crushing of circular and square tubes. *Int. J. Impact Engng* **2**, 263–281.

Abramowicz, W. and Jones, N. (1986). Dynamic progressive buckling of circular and square tubes. *Int. J. Impact Engng* **4**, 243–270.

Alexander, T. M. (1960). An approximate analysis of the collapse of thin cylindrical shells under axial loading. *Q. J. Mech. Appl. Math.* **13**, 10–15.

Allan, T. (1968). Experimental and analytical investigation of the behaviour of cylindrical tubes subjected to axial compressive forces. *J. Mech. Engng Sci.* **10**, 182.

Amdahl, J. and Soreide, T. H. (1981). Energy absorption in axially compressed cylindrical shells with special reference to bulbous bows in collision. *Norwegian Maritime Res.* **4**, 2–11.

Andrews, K. R. F., England, G. L. and Ghani, E. (1983). Classification of the axial collapse of cylindrical tubes under quasi-static loading. *Int. J. Mech. Sci.* **25,** 687–696.

Andronicou, A. and Walker, A. C. (1981). A plastic collapse mechanism for cylinders under uniaxial end compression. *J. Const. Steel Res.* **1,** 23–34.

Coppa, A. P. (1962). Collapsible shell structures for lunar loading. *General Electric Report TIS R625D9.* King of Prussia, PA.

Foppl, L. (1926). *Sitzsber. Math.-physik. Kl-bayer. Akad. Wiss.*, München, p. 27.

Geckeler, J. W. (1928). *Z. angew. Math. Mech.* **8,** 341.

Grzebieta, R. H. (1990). An alternative method for determining the behaviour of round stocky tubes subjected to an axial rush load. *Thin-Walled Struct.* **9,** 61–89.

Horton, W. H., Bailey, S. C. and Edwards, A. M. (1966). Nonsymmetric buckle patterns in progressive plastic buckling. *Exp. Mech.* **6,** 433–444.

Johnson, W. (1972). *Impact Strength of Materials.* Edwards Arnold, London.

Johnson, W., Soden, P. D. and Al-Hassani, S. T. S. (1977). Inextensional collapse of thin-walled tubes under axial compression. *J. Strain Anal.* **12,** 317.

Jones, N. (1989). *Structural Impact*, Cambridge University Press, Cambridge.

Mallock, A. (1908). Note on the instability of tubes subjected to end pressure and on the folds in a flexible material. *Proc. Roy. Soc., Series A* **81,** 388–393.

Reddy, T. Y. and Zhang, E. (1993). Effect of strain hardening on the behaviour of axially crushed cylindrical tubes. In *Advances in Engineering Plasticity and its Applications* (ed. W. B. Lee), Elsevier, London, pp. 755–762.

Singace, A. A., ElSobky, H. and Reddy, T. Y. (1995). On the eccentricity factor in the progressive crushing of tubes. *Int. J. Solids Struct.* **32,** 3589–3602.

Sobel, L. H. and Newman, S. Z. (1980). Plastic buckling of cylindrical shells under axial compression. *Trans. ASME, J. Press. Vess. Tech.* **102,** 40–44.

Wierzbicki, T., Bhat, S. U. (1984). A moving hinge solution for axisymmetric crushing of tubes. *Int. J. Mech. Sci.* **28,** 135–151.

Wierzbicki, T., Bhat, S. U., Abramowicz, W. and Brodkin, D. (1992). Alexander revisited—a two folding elements model of progressive crushing of tubes. *Int. J. Solids Struct.* **29,** 3269–3288.